Post-processing the U.S. National Water Model with a Long Short-Term Memory Network

Journal:	*Journal of the American Water Resources Association*
Manuscript ID	Draft
Manuscript Type:	Technical Paper
Date Submitted by the Author:	n/a
Complete List of Authors:	Frame, Jonathan; University of Alabama, Geological Sciences Nearing, Grey; University of Alabama, Geological Sciences Kratzert, Frederik; Johannes Kepler University, LIT AI Lab & Institute for Machine Learning Raney, Austin; University of Alabama, Geography Rahman, Mashrekur; University of Alabama, Geological Sciences
Key Terms:	streamflow < HYDROLOGY, National Water Model, long short-term memory, post-processing

Post-Processing the U.S. National Water Model with a Long Short-Term Memory Network

Jonathan M. Frame, Grey S. Nearing, Frederik Kratzert, Austin Raney, and Mashrekur Rahman

Department of Geological Sciences, University of Alabama, Tuscaloosa, AL USA (Frame & Rahman); Upstream Tech, Natel Energy Inc. Alameda, CA USA (Nearing); LIT AI Lab & Institute for Machine Learning, Johannes Kepler University, Linz, Austria (Kratzert); Department of Geography, University of Alabama; Tuscaloosa, AL USA (Raney).

(Correspondence to Frame: jmframe@crimson.ua.edu)

Research Impact Statement: Post-processing the U.S. National Water Model with deep learning improves the mean daily streamflow predictions. Deep learning predictions gain physical realism from the NWM inputs. This work advances theory-guided machine learning for large scale hydrological modeling.

ABSTRACT: U.S. National Water Model (NWM) daily averaged streamflow predictions were post-processed with a long short-term memory (LSTM) deep learning network. The LSTM post-processor provided a significant benefit to nearly all aspects of NWM daily averaged streamflow predictions. Adding NWM states and fluxes as dynamic inputs to the LSTM improves the representation of physical streamflow patterns. The NWM is a large scale, process-based and physics-based, hydrology simulator. Although NWM achieves coupling of multi-scale hydrological processes, its predictability at individual catchments can be improved. Hydrologic post-processing is an approach to reduce systematic simulation errors with statistical models, and has been shown to improve forecast accuracy of both calibrated and uncalibrated models. In this experiment we trained a LSTM network to post-process the NWM output, and tested performance at 531 basins across the continental United States. Additional results are presented for performance by region, calibrated vs. uncalibrated basins, and for different dynamic training input sets for the LSTM network.

(KEYWORDS: National Water Model; theory-guided machine learning; long short-term memory; streamflow.)

Submitted to the Journal of The American Water Resources Association (JAWRA)

INTRODUCTION

The U.S. National Water Model (NWM), based on WRF-Hydro (Cosgrove *et al.,* 2015), is an emerging large-scale hydrology simulator with 2.7 million river reaches. Some specific details of the NWM advancements in large scale hydrology are described by Elmer (2019, page 11), including increased resolution and number of stream reaches for a model covering the continental United States (CONUS). A strength of WRF-Hydro is simulating hydrologic dynamics (timing of the response) (Salas *et al.*, 2018). The NWM is a useful tool in terms of hydrology over large spatial domains, but the performance has been shown to vary widely (Hansen *et al.*, 2019). Hansen *et al.* (2019) evaluated the performance of the NWM in the Colorado River Basin in terms of drought and low flows; they found better performance in the upper basin than the lower basin, and attributed the discrepancy to the NWM's success simulating snowpack hydrology. WRF-Hydro's performance at a regional scale shows poor performance in the Southwest and Northern Plains (Salas *et al.*, 2018). Sources of error in WRF-hydro may come from lakes, reservoirs, floodplain dynamics and soil parameter calibration (Salas *et al.*, 2018).

The NWM version 2.0 is calibrated at 1,457 basins within the large-scale domain of CONUS. The USGS records daily streamflow at 28,529 basins (https://nwis.waterdata.usgs.gov/nwis, accessed June 2020). Calibrating the model at each stream gauge within the NWM domain would be a prohibitively large computational expense. Regionalizing calibrated basins can be used to improve forecast accuracy without having to calibrate each individual basin, but the accuracy in problematic regions would suffer (*e.g.*, Lower Colorado River and the Southwest). In the current stage of the NWM development the community should seek efficient and robust techniques to 1) make the best forecasts possible,

Submitted to the Journal of The American Water Resources Association (JAWRA)

and 2) maintain an agility and adaptability to future research which may continually increase forecast quality. There are promising results in the data science realm that may be directly (and immediately) applicable to the NWM.

Machine learning (ML) is gaining popularity in hydrological science, and there has been a call to merge ML with traditional hydrological modeling (Reichstein *et al.*, 2019). The "long short-term memory" network (LSTM) (Hochreiter, 1991; Hochreiter and Schmidhuber, 1997) is a time series deep learning method that is particularly well suited to model hydrologic processes (Kratzert *et al.*, 2018). LSTMs have been effective at simulating predictions of surface runoff at the daily time scale (Kratzert *et al.*, 2019a), including in ungauged catchments where traditional methods of calibration do not work (Kratzert *et al.*, 2019b). One potential problem with ML, however, is that it lacks a physical basis. While there are emerging efforts in hydrology to merge physical understanding with machine learning (Karpatne *et al.*, 2017a; Daw *et al.*, 2020; Pelissier *et al.*, 2019; Chadalawada *et al.*, 2020; Tartakovsky *et al.*, 2020), *theory informed machine learning* (Karpatne *et al.*, 2017b) is still relatively immature in hydrology.

Hydrologic post-processing is a straightforward theory-informed machine learning approach which avoids the problems of calibration across large spatial domains. This approach can remove systematic errors in the model prediction, and has been shown to improve forecast accuracy of both calibrated and uncalibrated basins, particularly in wet basins (Ye *et al.*, 2014). The general methodology of post-processing involves taking the output of a process-based model and feeding it into a data-driven model. We suggest an immediate step for improving NWM forecast accuracy without the computational expense of calibration is post-processing streamflow predictions with ML. In this paper we apply a LSTM-based post processor for the NWM to improve basin-scale streamflow predictions.

Submitted to the Journal of The American Water Resources Association (JAWRA)

The LSTM post-processor was applied to 531 basins across the CONUS. The basins chosen for this large-scale analysis are mostly without engineered control structures, such as dams, canals, and levees. This was a deliberate choice made for the purpose of simulating a close-to-natural rainfall-runoff response. Our goal is to learn about basin-scale rainfall-runoff processes, rather than the hydraulic engineering implications resulting from simulated controlled flow, *e.g.* a reservoir release. Kim *et al.* (2020) showed the limitation of the NWM to predict streamflow in a highly engineered watershed and the need for representing controlled releases. Thus, we are using some of the simplest, and top performing, applications of the NWM for these experiments.

METHODS

Data & Models

CAMELS Catchments. This study uses the Catchment Attributes and Meteorological dataset for Large Sample Studies (CAMELS) (CAMELS; Newman *et al.*, 2015; Addor *et al.*, 2017). These data have been curated by the US National Center for Atmospheric Research (NCAR; https://ral.ucar.edu/solutions/products/camels, accessed March 2020). We used 531 of the 671 basins - these were the same basins used by Newman *et al.* (2015), who excluded basins with large discrepancies in different methods for measuring basin area and also basins larger than 2,000 km^2. CAMELS data include corresponding daily streamflow records from United States Geological Survey (USGS) gauges, and meteorological forcing data (precipitation, max/min temperature, vapor pressure and total solar radiation) come from North American Land Data Assimilation System (NLDAS; Xia *et al.*, 2012).

Submitted to the Journal of The American Water Resources Association (JAWRA)

National Water Model. We used the National Water Model version 2.0 reanalysis, which contains output from a 25-year (January 1993 through December 2019) retrospective simulation (https://docs.opendata.aws/nwm-archive/readme.html, accessed June 2020). The NWM retrospective ingests rainfall and other meteorological forcings from atmospheric reanalyses (https://water.noaa.gov/about/nwm, accessed June 2020.). NWM output includes streamflow (point fluxes) and land surface (gridded) states and fluxes. The specific features that we used from the NWM output are shown in Table 1. To be compatible with the LSTM model, which uses a one-day timestep, we took the mean values across the UTC calendar day (12AM - 11PM) to produce daily records from the hourly NWM when used as input to the LSTM, but for NWM streamflow diagnostics we used the local calendar day (based on U.S. time zone) to be compatible with the USGS gauge records. Channel routing point data (CHRT) was collected at the NWM stream reach that corresponds to the stream gauge associated with each CAMELS catchment. Gridded land surface data (LDAS) was collected from each 1 km^2 Noah-MP cell contained within the boundaries of each CAMELS catchment, and these were averaged to produce a single representative (lumped) value for each catchment. Gridded routing data were similarly collected from each 250 m^2 cell, and we also included the maximum value within the catchment boundary. We did not include lake input and output fluxes because these would be inconsistent across basins (some basins have zero and some basins have multiple lakes). Note that the units of the NWM outputs are not required for the LSTM post-processor.

TABLE 1. National Water Model Output Data

Feature name	Feature	Resolution
ACCET	Accumulated evapotranspiration	1Km
FIRA	Total net long-wave (LW) radiation to atmosphere	1Km
FSA	Total absorbed short-wave (SW) radiation	1Km
FSNO	Snow cover fraction on the ground	1Km
HFX	Total sensible heat to the atmosphere	1Km

LH	Latent heat to the atmosphere	1Km
SNEQV	Snow water equivalent	1Km
SNOWH	Snow depth	1Km
SOIL M	Volumetric soil moisture	1Km
SOIL W	Liquid volumetric soil moisture	1Km
TRAD	Surface radiative temperature	1Km
UGDRNOFF	Accumulated underground runoff	1Km
streamflow	River Flow	point
q_lateral	Runoff into channel reach	point
velocity	River Velocity	point
qSfcLatRunoff	Runoff from terrain routing	point
qBucket	Flux from groundwater bucket	point
qBtmVertRunoff	Runoff from bottom of soil to groundwater bucket	point
sfcheadsubrt	Ponded water depth	250Km
zwattablrt	Water table depth	250Km

Long short-term memory network. The LSTM takes two types of inputs: daily meteorological forcings and static catchment attributes. Again, note that the units of the forcing data are irrelevant when used as inputs for the LSTM, which does not include a mass or energy balance. We used eighteen catchment attributes from the CAMELS dataset related to climate, vegetation, topography, geology, and soils. These are described in more detail by Addor *et al.* (2017) and listed here in Table 2. Catchment attributes are static for each basin (do not change in time). We trained the LSTM with the features described in Table 1 of Kratzert *et al.* (2019b). For a detailed explanation of the LSTM itself see Kratzert *et al.* (2018).

TABLE 2. LSTM Inputs

Meteorological Forcing Data	
Maximum Air Temp (TMax)	2-meter daily maximum air temperature [C]
Minimum Air Temp (TMin)	2-meter daily minimum air temperature [C]
Precipitation (PRCP)	Average daily precipitation [mm/day]
Radiation (SRAD)	Surface-incident solar radiation [W/m^2]
Vapor Pressure (Vp)	Near-surface daily average [P_a]
Static Catchment Attributes	
Precipitation Mean	Mean daily precipitation
PET Mean	Mean daily potential evapotranspiration
Aridity Index	Ratio of Mean PET to Mean Precipitation
Precipitation Seasonality	Estimated by representing annual precipitation and temperature as sin waves

Submitted to the Journal of The American Water Resources Association (JAWRA)

	Positive (negative) values indicate precipitation peaks during the summer (winter). Values of approx. 0 indicate uniform precipitation throughout the year.
Snow Fraction	Fraction of precipitation falling on days with temp [C].
High Precipitation Frequency	Frequency of days with ≤ 5x mean daily precipitation. Average duration of high precipitation events (number of consecutive days with ≤ 5x mean daily precipitation).
Low Precipitation Frequency	Frequency of dry days (< 1 mm/day).
Low Precipitation Duration	Average duration of dry periods (number of consecutive days with precipitation < 1 mm/day).
Elevation	Catchment mean elevation.
Slope	Catchment mean slope.
Area	Catchment area.
Forest Fraction	Fraction of catchment covered by forest.
LAI Max	Maximum monthly mean of leaf area index.
LAI Difference	Difference between the max. and min. mean of the leaf area index.
GVF Max	Maximum monthly mean of green vegetation fraction.
GVF Difference	Difference between the maximum and minimum monthly mean of the green vegetation fraction.
Soil Depth (Pelletier)	Depth to bedrock (maximum 50m).
Soil Depth (STATSGO)	Soil depth (maximum 1.5m).
Soil Porosity	Volumetric porosity.
Soil Conductivity	Saturated hydraulic conductivity.
Max Water Content	Maximum water content of the soil.
Sand Fraction	Fraction of sand in the soil.
Silt Fraction	Fraction of silt in the soil.
Clay Fraction	Fraction of clay in the soil.
Carbonate Rocks Fraction	Fraction of the catchment area characterized as “carbonate sedimentary rocks”.
Geological Permeability	Surface permeability (log10).

For the post-processing runs we added the states, fluxes, and streamflow predictions from version 2.0 of the NWM. We trained the LSTM on water years 2004 through 2014 and tested the predictions on out-of-sample water years 1994 through 2002. The LSTM uses a 365-day LSTM look-back period, so a full year gap was left between training and testing to prevent bleedover (*i.e.* information exchange) between the two periods. We trained separate LSTMs with ten unique random seeds for initializing weights and biases, and calculated benchmarking statistics using the ensemble mean hydrograph. The LSTM makes predictions representing runoff in units [mm], reflecting an area normalized volume of water that moves through a stream at each model timestep. USGS gauge records (and the NWM predictions) are in streamflow units [m^3/s]. We

Submitted to the Journal of The American Water Resources Association (JAWRA)

used the geospatial fabric estimate of the catchment area provided in the CAMELS dataset to convert all streamflow to units [mm] for our diagnostic comparison.

Experimental Design

A simple schematic of the LSTM used as a post-processor for the NWM streamflow prediction is shown in Figure 1. The LSTM post-processor takes the NWM outputs as inputs, and the result is a LSTM-based streamflow prediction that is influenced by the process-based NWM. This is a straightforward method of theory-guided machine learning, which will combine the predictability of ML with the robustness and physical realism of process-based modeling.

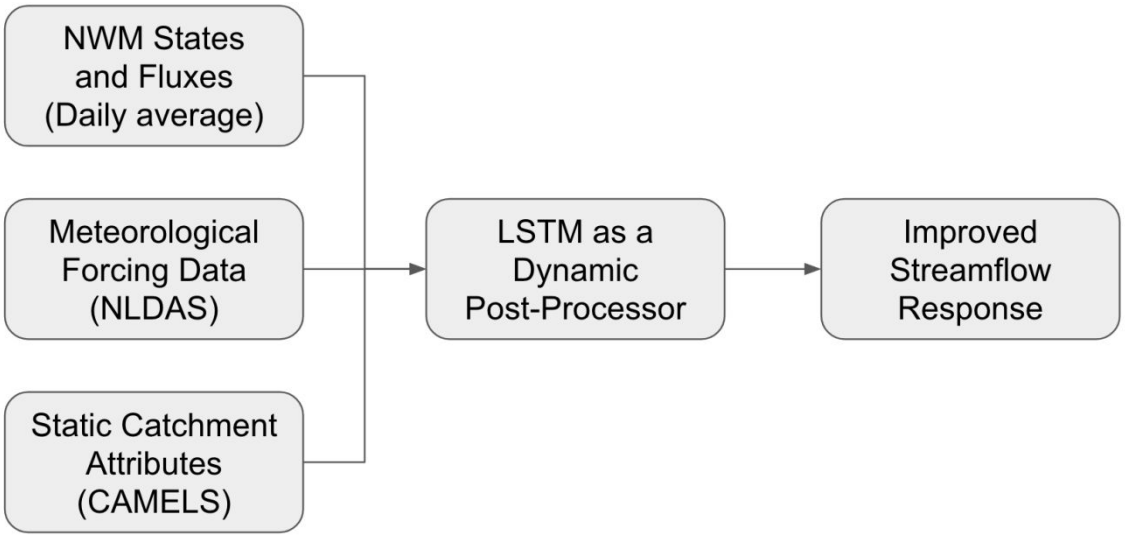

FIGURE 1. Flow chart showing the LSTM used as a post-processor for the NWM streamflow prediction.

As a quality check, we compared the results from each LSTM ensemble member, and found a relative standard error of the mean streamflow about 1%, and relative standard error of the Nash-Sutcliffe Efficiency (NSE) value of about 0.01%. This means that all LSTM solutions are similar between random initialization seeds. Gauch *et al.* (2019) attributed a 0.01 discrepancy in NSE values of the LSTM predictions to non-determinism of the loss function minimization. In

Submitted to the Journal of The American Water Resources Association (JAWRA)

our experiments discrepancies in the loos function occur between different random seed initializations, but running the training procedure twice with the same random seed gives an identical solution, satisfying the definition of determinism.

Performance metrics. We calculated a number of metrics for a robust evaluation of the predictive performance, including the NSE and Kling-Gupta Efficiency (KGE) values (Ritter and Muñoz-Carpena, 2013). The variance, bias and Pearson correlation metrics were calculated separately as components of the NSE (Gupta *et al.*, 2009); these tell us about relative variability, mass conservation and linear correlation between the modeled/observed streamflow values, respectively. The metrics were calculated in two ways: 1) at each basin and then averaged together, and 2) using all of the flows from all basins combined.

Our graphical results focus on three performance metrics: (i) NSE measures the overall predictive performance as a correlation coefficient for the 1:1 linear fit between simulations and observations, (ii) Peak timing error measures the absolute value of differences (in units days) between simulated and observed peak flows for a given event, and (iii) total bias measures the overall bias of the simulated hydrograph relative to observations and represents how well the model matches the total volume of partitioned rainfall that passes through the stream gauge at each basin.

We also calculated performance metrics on different flow regimes. Rising limbs and falling limbs were characterized by a one-day derivative, where positive derivatives were categorized as rising limb, and negative derivatives as falling limb. High flows were characterized as all flow above the 80th percentile in a given basin, and low flows as below the 20th percentile in a given basin.

We tested the performance of the LSTM post-processor in different regions. We split the basins by USGS designated "water resource regions" (https://water.usgs.gov/GIS/regions.html, accessed July 2020). To analyze the regions individually we averaged the NSE, bias and timing error of the CAMELS basins within each region.

We set an alpha value for statistical significance to $\alpha = 0.05$. To control for multiple comparisons we adjusted the alpha values using family-wise error rate equal to $1-(1-\alpha)^m$, with m being the number of significance tests (86 in total), which brought our effective alpha value down to 0.049. We tested for statistical significance with a Wilcoxon signed-rank test against the null hypothesis that our test model (LSTM post-processor) performance across basins came from the same distribution as our base models (NWM and LSTM).

Simulated hydrograph representation of hydrologic signatures. Hydrologic signatures help us understand how well a model represents important aspects of real-world streamflow, and where improvement should be made to the model's conceptualization (Gupta *et al.*, 2008). We analyzed the hydrologic signatures described by Addor *et al.* (2018), and these are listed below in Table 3. We calculated the true signatures with USGS streamflow observations, and calculated model representations with predicted values of daily streamflow. The comparison between true values and predicted values was made with the correlation coefficient (r^2), higher values indicating better representation of hydrologic signature across basins by the model. We used the Steiger method to test for statistically significant improvement (or detriment) between the base models and the LSTM post-processor (Steiger and Browne, 1984).

TABLE 3. Hydrologic signatures (adapted from Addor *et al.* 2018)

Signature description	Signature name
Average duration of low-flow events	low_q_dur
Frequency of days with zero flow	zero_q_freq

Submitted to the Journal of The American Water Resources Association (JAWRA)

Average duration of high-flow events	high_q_dur
Streamflow precipitation elasticity	stream_elas
Frequency of high-flow days	high_q_freq
Slope of the flow duration curve	slope_fdc
Frequency of low-flow days	low_q_freq
Baseflow index	baseflow_index
Runoff ratio	runoff_ratio
Mean half-flow date	hfd_mean
5 percent flow quantile	q5
95 percent flow quantile	q95
Mean daily discharge	q_mean

Identifying basins best suited for post-processing with Random Forest regression. The LSTM post-processor did not improve performance at every basin. It is therefore valuable to know if the LSTM post-processor will work in any particular basin before implementation. We trained a random forest regression to predict the performance change between the LSTM and the LSTM post-processor at each individual basin. The inputs to the regression analysis were the performance score of the NWM streamflow predictions, hydrologic signatures and catchment characteristics. These regressors are useful to help interpret what basins might benefit most from the LSTM post-processor. We trained and tested random forests using k-fold cross-validation with 20 splits (k=20) over the 531 basins. We report the correlation (r^2) of out-of-sample random forest predictions of post-processing improvements vs. real post-processing improvements. We also calculated the mean decrease in impurity (or Gini importance) to determine the total reduction of the criterion brought by each feature.

Interpretation of LSTM with integrated gradients. We calculated integrated gradients (Sundararajan *et al.*, 2017) to attribute the LSTM inputs (both atmospheric forcings and NWM outputs) to the total prediction of streamflow. Integrate gradients are a type of sensitivity analysis

Submitted to the Journal of The American Water Resources Association (JAWRA)

that are relatively insensitive to low gradients (*e.g.*, at the extremes of neural network activation functions). Integrated gradients are calculated separately for each input, at each timestep, for each lookback timestep, in each basin. This means that for 9 years of test data with a 365-day lookback there are about 1.2 million integrated gradients per input, per basin.

Interpretation of LSTM with correlations between performance and NWM inputs. We made a direct connection between LSTM post-processor improvements with the NWM outputs using correlation. We calculated Pearson R values between the basin average value of each NWM input feature and the total performance change (NSE, bias and peak timing). These correlations were calculated for different flow regimes (all flows, rising/falling limbs, and high/low flows. The strengths of these correlations (positive or negative) indicate which types of basins (via NWM features) are benefiting most from the LSTM post-processor.

Splitting the CAMELS catchments by calibrated / uncalibrated. Of the NWM calibrated basins, 480 overlap with the 531 CAMELS catchments we are using in this study. In a separate set of experiments, we trained the LSTM (and the LSTM post-processor) on only the 480 calibrated basins. We then used the full set of 531 catchments to test the performance out-of-sample. We analyzed the 480 in-sample basins and 51 out-of-sample basins separately using the NSE, bias and timing error metrics.

Training the LSTM with only the NWM states and fluxes. To complete this post-processing analysis, we performed a separate set of experiments having trained the LSTM (to predict streamflow) using only the NWM states and fluxes as dynamic inputs (all static catchment attributes were still used, but the five atmospheric forcings were left out). We also performed this experiment with only the NWM states (soil moisture, groundwater, total radiation

Submitted to the Journal of The American Water Resources Association (JAWRA)

and snow states). We analyzed these sets of runs using the NSE, bias and peak timing error. This provides an additional sensitivity analysis to the NWM states and fluxes.

RESULTS

Predictive performance

Post-processing the NWM with LSTMs significantly improved predictive performance. Figure 2 shows the cumulative distributions of three performance metrics (NSE, peak timing error, and total bias). Figure 2 also shows scatter plots comparing the performance of different models and includes r^2 values.

Submitted to the Journal of The American Water Resources Association (JAWRA)

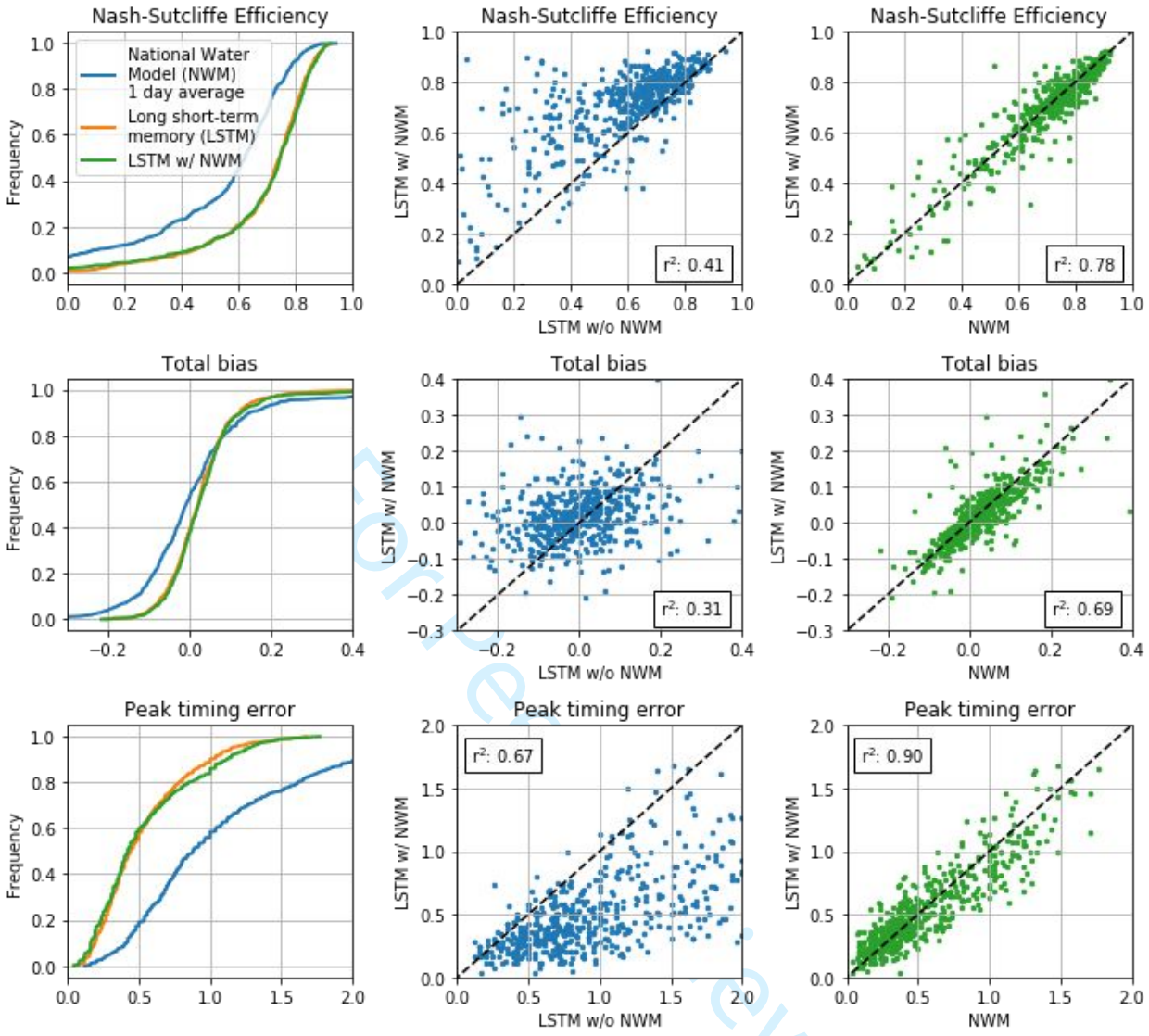

FIGURE 2. Results showing the cumulative distributions of model performance calculated as Nash-Sutcliffe Efficiency (NSE), total bias and peak timing error over a 10-year test period in 531 CAMELS catchments. The National Water Model (NWM) reanalysis streamflow is averaged daily, long short-term memory (LSTM) networks are plotted with the original inputs (w/o NWM), and the LSTM w/ NWM represents the machine learning post-processed LSTM model with NWM inputs.

The LSTM post-processor improved the NSE score of the NWM mean daily streamflow at a total of 488 (92%) and reduced accuracy in 43 basins (8%) of the total 531 CAMELS basins. The LSTM post-processor improved the total bias of the NWM mean daily streamflow at a total

Submitted to the Journal of The American Water Resources Association (JAWRA)

of 331 (62%) of basins and improved the peak timing error at a total of 494 (93%) of basins. Improvements to performance in each basin are plotted spatially in Figure 3.

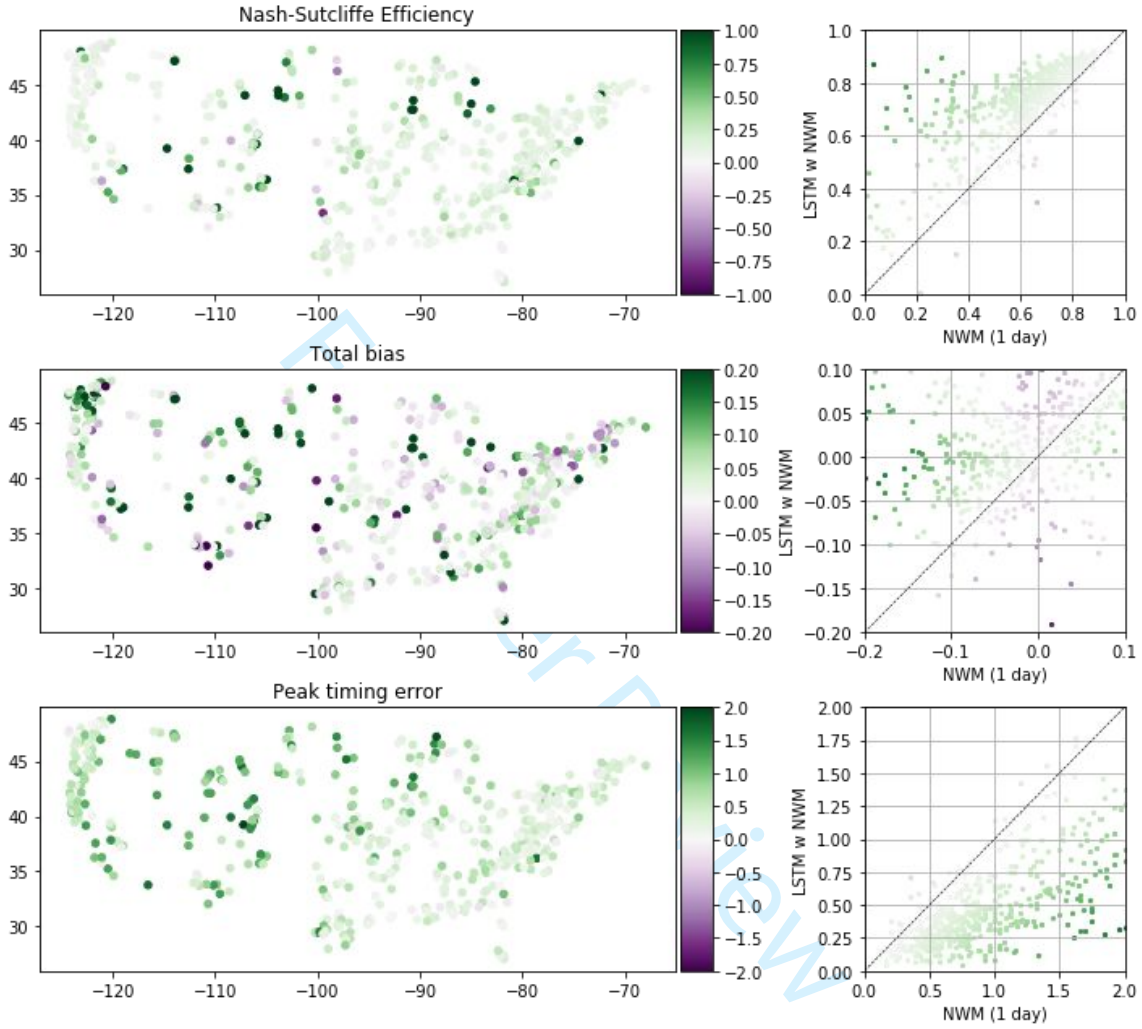

FIGURE 3. Improvements due to post-processing vs. the NWM in 531 CAMELS basins across CONUS. Green indicates basins where post-processing improved performance over the NWM (darker indicates larger relative improvement), and purple indicates basins where there was a decrease in performance (darker indicating worse relative detriment).

The LSTM post-processor improved predictions from the standalone LSTM in about half of the basins. The NSE score increased in a total of 291 (55%) and decreased in 240 basins (45%) of the 531 basins. Total bias improved in 258 (49%) of the basins. Peak timing improved

in 228 (43%) and was a detriment in 228 (43%) of the basins. Performance improvements relative to the standalone LSTM are plotted spatially in Figure 4.

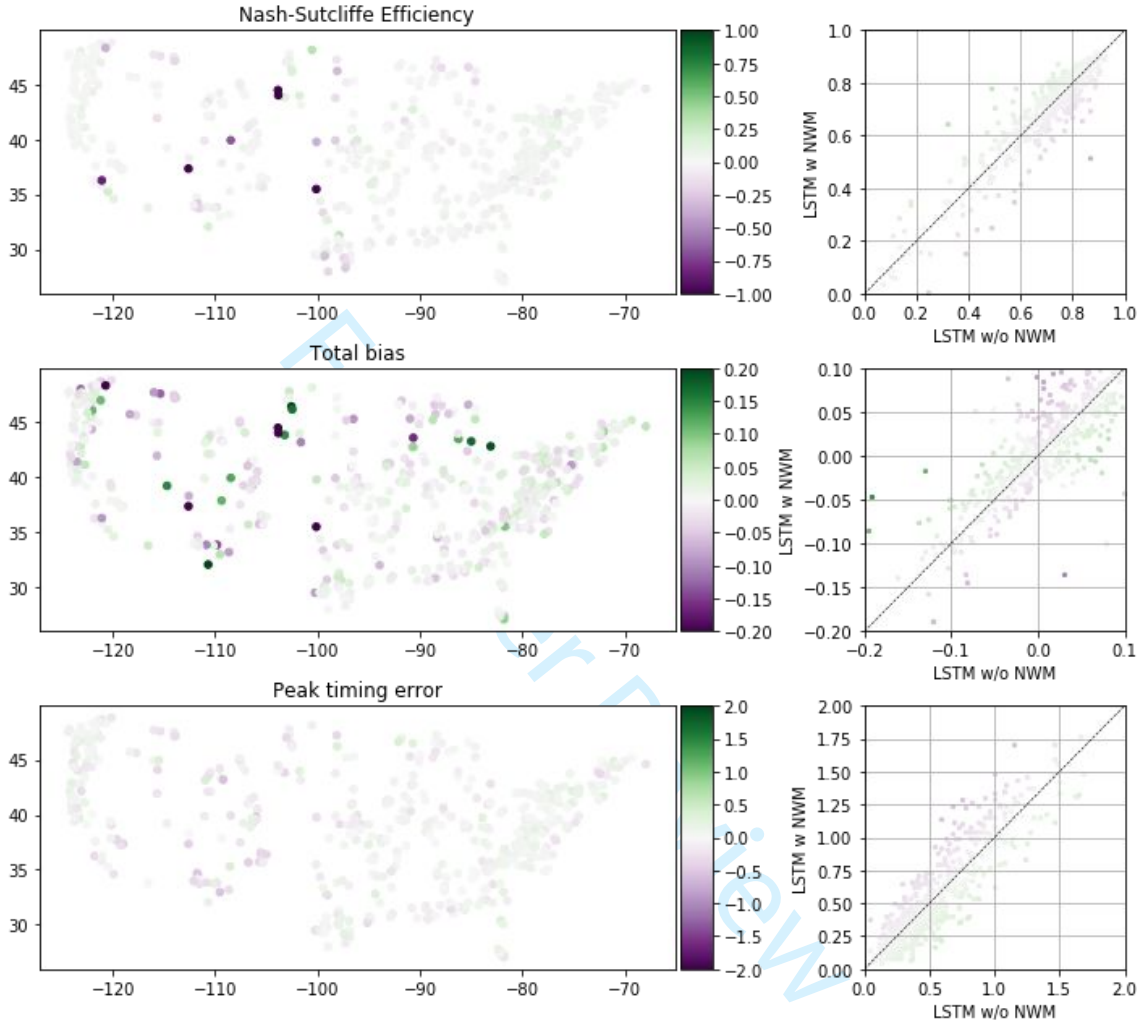

FIGURE 4. Improvements due to adding NWM states and fluxes as inputs into an LSTM in 531 CAMELS basins across CONUS. Green indicates basins where post-processing improved performance over the LSTM without NWM inputs (darker indicates larger relative improvement), and purple indicates basins where there was a decrease in performance (darker indicating worse relative detriment).

Performance by flow regime

Submitted to the Journal of The American Water Resources Association (JAWRA)

The LSTM post-processor improved predictive performance of the NWM according to the NSE and KGE metrics, as well as their components (variance and correlation). A full set of performance metrics broken down by flow regime are shown in Table 4. The left side of the table shows the average of metrics calculated individually at each basin, and the right side of the table shows the metrics as calculated combining the flows from all basins. The NSE includes both mean and median averages, but the rest of the metrics are only averaged by median. Failure to reject the null hypothesis of significance (that the test model, LSTM post-processor, is different from the base models, NWM & LSTM) is denoted by an asterisk.

TABLE 4. Predictive performance for NWM, LSTM alone and the LSTM Post-processed NWM during various flow regimes. The Nash-Sutcliffe Efficiency (NSE) and Kling-Gupta Efficiency (KGE) are overall performance metrics of prediction quality. Variance, bias and correlation (R) are the components of the NSE. We calculated these in two ways: 1) calculated at each basin, then averaged across all basins, and 2) calculated once using the values from all basins combined. Note that calculations done once across all basins does not include a test of significance.

Flow categories	**Calculated per-basin**						**All basins**			
All flows	**NSE (mean)**	**NSE (median)**	**KGE**	**variance**	**bias**	**R**	**NSE**	**variance**	**bias**	**R**
NWM	0.46	0.62	0.64	0.82	-0.01	0.82	0.75	0.85	-0.02	0.87
LSTM	0.69	0.74	0.74	0.83	0.02	0.88	0.82	0.89	0.01	0.90
LSTM+NWM	0.67	0.75	0.76	0.87	0.02	0.88	0.82	0.93	0.02	0.91
Rising limbs	**NSE (mean)**	**NSE (median)**	**KGE**	**variance**	**bias**	**R**	**NSE**	**variance**	**bias**	**R**
NWM	0.47	0.60	0.60	0.77	-0.07	0.81	0.73	0.82	-0.05	0.85
LSTM	0.66	0.71	0.72	0.80	-0.01	0.86	0.78	0.85	-0.01	0.88
LSTM+NWM	0.65	0.72	0.74	0.85	0.00	0.87	0.79	0.89	0.00	0.89
Falling limbs	**NSE (mean)**	**NSE (median)**	**KGE**	**variance**	**bias**	**R**	**NSE**	**variance**	**bias**	**R**
NWM	0.28	0.60	0.64	0.94	0.04	0.83	0.78	0.90	0.00	0.88
LSTM	0.69	0.78	0.77	0.92	0.05	0.90	0.87	0.96	0.03	0.93
LSTM+NWM	0.65	0.77	0.77	0.94	0.05	0.90	0.87	0.98	0.03	0.93
Above 80th percentile	**NSE (mean)**	**NSE (median)**	**KGE**	**variance**	**bias**	**R**	**NSE**	**variance**	**bias**	**R**
NWM	0.15	0.39	0.55	0.82	-0.12	0.72	0.69	0.83	-0.10	0.84
LSTM	0.53	0.58	0.67	0.81	-0.08	0.81	0.78	0.86	-0.06	0.88
LSTM+NWM	0.50	0.60	0.69	0.84	-0.07	0.81	0.79	0.90	-0.04	0.89
Below 20th	**NSE (mean)**	**NSE (median)**	**KGE**	**variance**	**bias**	**R**	**NSE**	**variance**	**bias**	**R**

percentile										
NWM	-18384.37	-17.47	-1.96	3.79	1.89	0.36	0.37	1.31	0.22	0.81
LSTM	-4749.68	-16.35	-1.31	2.85	3.27	0.43	0.56	1.26	0.33	0.89
LSTM+NWM	-5147.62	-14.66	-1.24	2.85	2.87	0.43	0.58	1.28	0.30	0.90

Note: blue indicates post-processing significantly helps the NWM

Note: pink indicates post-processing significantly hurts the NWM

In general Table 4 shows that the performance of the LSTM post-processor is an improvement over the NWM in nearly all flow regimes, and by most metrics. The LSTM post-processor also improves upon the LSTM at a majority of the basins, and by most metrics. The rising limb and high flow regimes were improved by the LSTM post-processor according to every metric.

Bias is the only metric that was reduced due to post-processing, and the difference was highest in low flow regimes. Flows below the 20th percentile are poorly predicted by all models. This is likely due to the fact that all models tend to have difficulty predicting zero streamflow, and the 101 basins with periods of zero streamflow are weighing down the average. This will be discussed further in terms of hydrologic signatures.

The right side of the table has better performance values than the average of metrics calculated individually at each basin. This is a result of some of the better performing basins compensating for poorer performing basins, or from a different perspective, some basins have relatively poor performance which weighs down the average.

Performance by region

Results of a regional analysis of performance are shown below in Table 5. The LSTM post-processor significantly improves the NSE in fifteen of the eighteen regions, the peak timing

Submitted to the Journal of The American Water Resources Association (JAWRA)

error in sixteen regions (all regions with enough basins for a statistical evaluation) and improves bias in only one region. Note that region 9 is represented by only two CAMELS basins, which is not satisfactory for statistical evaluation. The bias was better represented by the NWM than the post-processor in five of the eighteen basins, including the entire East Coast (regions 1, 2 & 3), the Pacific Northwest (17) and the Lower-Colorado River (15).

TABLE 5. Predictive performance for NWM, LSTM alone and the LSTM Post-processed NWM in different USGS water resources regions.

USGS Region	n	NSE		Total bias		Peak timing error	
		NWM	LSTM w/ NWM	NWM	LSTM w/ NWM	NWM	LSTM w/ NWM
1	22	0.62	0.78	-0.05	0.07	0.66	0.32
2	69	0.49	0.74	0.03	0.03	0.63	0.29
3	79	0.56	0.71	0.02	-0.02	0.77	0.49
4	30	0.41	0.69	0.00	0.05	1.17	0.64
5	35	0.63	0.74	-0.04	0.03	0.62	0.35
6	16	0.70	0.80	-0.01	0.00	0.66	0.24
7	29	0.46	0.71	0.11	0.09	1.11	0.50
8	7	0.61	0.67	0.01	-0.03	0.81	0.63
9	2	0.29	0.40	-0.16	0.09	2.38	1.29
10	49	-0.06	0.46	0.14	0.08	1.64	0.88
11	22	0.31	0.56	0.05	0.04	1.06	0.60
12	32	0.28	0.33	-0.01	-0.01	1.13	0.61
13	7	0.24	0.63	0.16	0.09	2.15	1.17
14	15	0.50	0.74	-0.03	0.01	2.11	1.01
15	14	-0.02	0.33	-0.02	0.12	1.60	0.94
16	5	0.22	0.71	-0.05	-0.03	1.83	0.89
17	72	0.67	0.81	-0.03	0.04	1.08	0.46
18	26	0.59	0.74	-0.03	0.00	1.34	0.58

Post-Processing significantly helps the NWM
Post-Processing significantly hurts the NWM

Random Forest regression

Submitted to the Journal of The American Water Resources Association (JAWRA)

We assessed the LSTM post-processor's potential for improving predictions over the NWM at each individual basin. Figure 5 shows the results predicting the post processor improvement at each basin with an r^2 value of 0.82 between the true values and the predicted values. The strength of this prediction is heavily weighted by the outlier basins with abnormally large performance improvements from the post-processor. This means that the LSTM post-processor can improve the predictions in the basins where the NWM does most poorly.

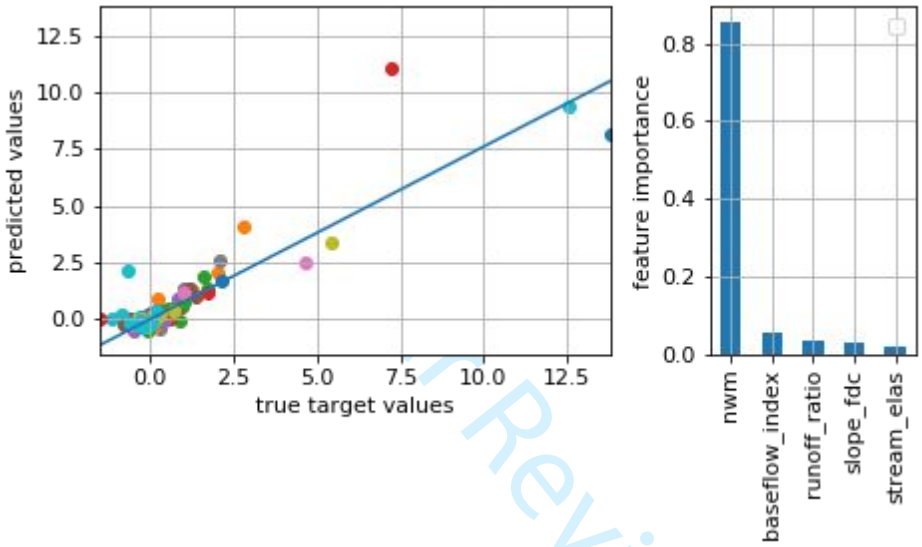

FIGURE 5. Predicting the LSTM post-processor improvement at each basin from with a random forest regression using NWM performance and hydrologic signatures as inputs. Left: Scatter plots for each of the 20 k-fold validation splits. Right: Average feature importance (across k-fold splits) on the prediction.

Figure 5 also shows the (Gini) importance of each regression. The r^2 value was the same with all hydrologic signatures included in the regression as it was with only the top four importance-ranked signatures (full analysis not shown). This figure shows the results when only those four signatures were used. The baseflow index is the signature with the highest importance for predicting if the LSTM post-processor will be beneficial.

Submitted to the Journal of The American Water Resources Association (JAWRA)

The aim of these results is to understand whether it is possible to identify basins where post-processing might be beneficial. Although we found relatively high predictability in the improvement expected from post-processing, a problem is that we required knowing ahead of time the NWM performance to do so. This prevents us from predicting post-processing improvement in *ungauged* basins, since calculating the NWM performance requires streamflow observations. Without the NWM performance as a predictor in this regression we achieved a r^2 value of 0.37 using all the hydrologic signatures and all the static catchment attributes together, shown in Figure 6. A total of 45 catchment attributes and signatures were included as regression inputs, but the figure shows only the Gini importance of the top five. The baseflow index is again the most important signature for the regression, and the second signature being the slope of the flow duration curve. The basin area is the most important catchment characteristic, followed by the mean basin area and basin elevation.

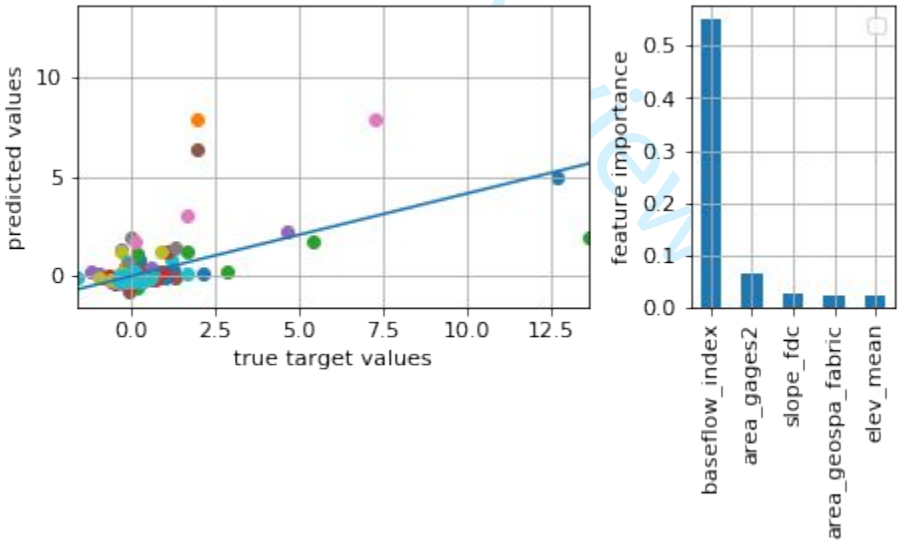

FIGURE 6. Predicting the LSTM post-processor improvement at each basin from with a random forest regression using static catchment attributes and hydrologic signatures as inputs. Left: Scatter plots for each of the 20 k-fold validation splits. Right: Top features ordered by Gini importance (averaged across k-fold splits) on the prediction.

Submitted to the Journal of The American Water Resources Association (JAWRA)

Integrated gradients

Figure 7 shows the relative strength of the total attribution of the dynamic inputs to the LSTM post processor averaged across the entire validation period and across each basin. The ordered magnitudes of the integrated gradients can be interpreted as corresponding to the order of importance of inputs. The most important dynamic features for the LSTM post-processor were: (i) precipitation from NLDAS, and (ii) routed streamflow from the NWM point data. Precipitation inputs were weighted higher than the NWM streamflow output itself, which means that even when NWM streamflow data were available, the LSTM learned to get information directly from forcings rather than from the NWM streamflow output. This indicates that the LSTM post-processor generates a new rainfall-runoff relationship rather than relying on the NWM, which makes some sense given the overall results (Figure 1) that show similar performance between the LSTM with and without NWM inputs.

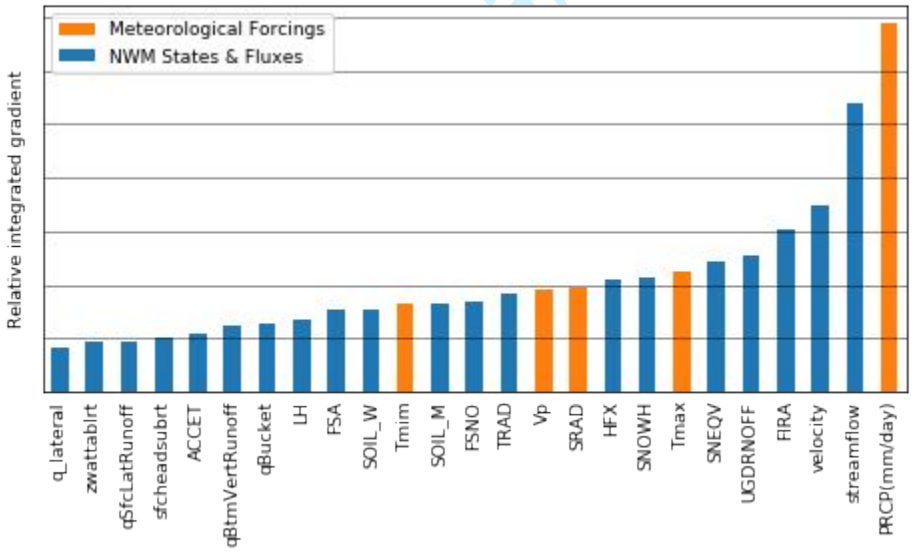

FIGURE 7. Attributions to the LSTM post-processor predictions. The vertical axis shows the relative magnitude of attribution (importance) for each input, with precipitation (PRCP) as the top contributor and NWM-predicted runoff into channel reach (q_lateral) contributing the least.

Submitted to the Journal of The American Water Resources Association (JAWRA)

Correlations between NWM inputs and improvements

Figure 8 shows correlations (over 531 basins) between the time-averaged NWM inputs and changes in NSE scores of the LSTM post-processor relative to both the LSTM alone and NWM alone. These correlations were calculated using the whole hydrograph. Results for rising limbs and falling limbs of the hydrograph were qualitatively similar to this figure, and were therefore omitted. The rows of this figure show that correlation was weaker for differences in NSE score than total bias and peak timing error. Performance differences between the NWM and the LSTM post-processor were most strongly (anti)correlated with stream velocity and underground runoff: basins with lower stream velocity (velocity) and less underground runoff (UGDRNOFF) saw greater performance improvement from (daily) post-processing. This means that in basins with high underground runoff and/or high stream velocity the LSTM post-processor improvements are smaller. In contrast, basins with higher total radiation (TRAD) and higher latent heat flux (LH) saw greater improvement due to post-processing. This means that in basins with more radiation and heat flux the LSTM post-processor improvements are larger. A direct interpretation of this could be that a flat meandering stream in the Southwest will benefit from the LSTM post-processor, which is consistent with the findings of Salas *et al.* (2018). Performance differences between the LSTM alone and the LSTM post-processor were most strongly correlated with snow water equivalent and snow depth. This is consistent with the findings of Hansen *et al.* (2019) that the NWM represents snowpack hydrology well.

Submitted to the Journal of The American Water Resources Association (JAWRA)

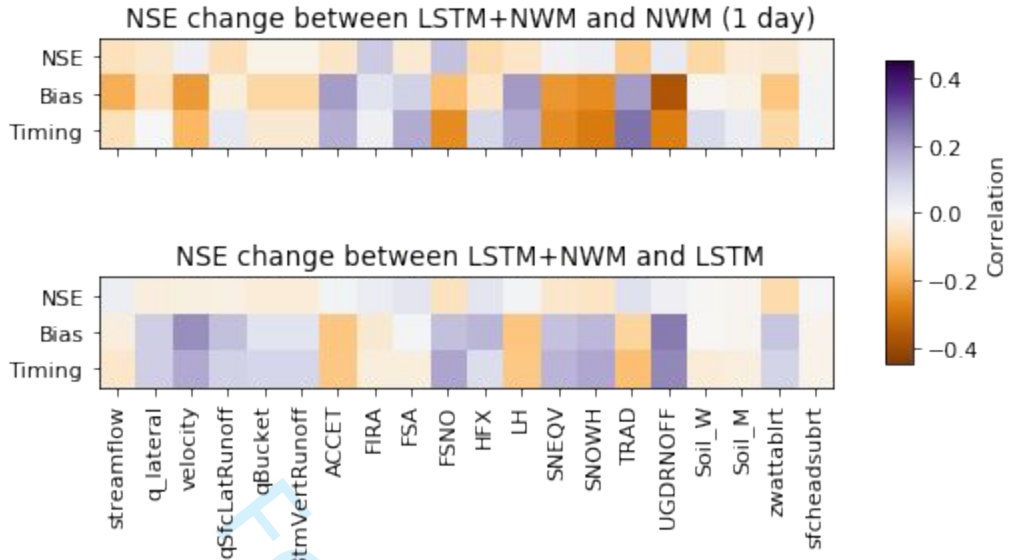

FIGURE 8. Correlations between the time-averaged NWM related inputs vs. NSE differences between the LSTM post-processor and both control models (LSTM alone and NWM alone).

Representations of hydrologic signatures

Results of the analysis of hydrologic signature representation are shown in Figure 9, which also shows that the hydrologic signatures that at best represented by the NWM are similarly the best represented by the LSTM post-processor, and the same is true for the poorly represented hydrologic signatures. The overall r^2 values averaged across all signatures for the NWM, LSTM and LSTM post-processor were 0.59, 0.60 and 0.61, respectively.

Submitted to the Journal of The American Water Resources Association (JAWRA)

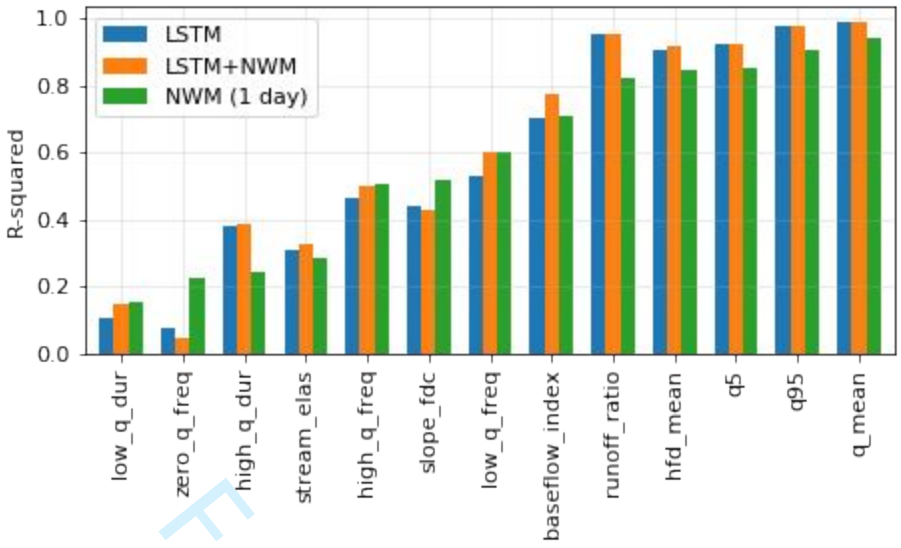

FIGURE 9. This plot shows the average representation of catchment hydrologic signatures by the NWM (blue), LSTM (orange) and the LSTM post-processor (green). The bars with the largest values represent the best performance. The signatures are ordered by their representation by the NWM.

The LSTM post-processor hurts the representation of the frequency of days with zero flow. There are 101 basins with any periods of zero flow. None of these models do well simulating zero flow, but the NWM is better at handling this situation, predicting zero flow periods at 56 basins. The LSTM and LSTM post-processor only predict periods of zero flows at 35 and 29 basins, respectively. This is an important characteristic in basins in the Southwest, where the NWM could use the benefit of the LSTM post-processor, so this would be a good place to focus future research of theory-guided ML for hydrology.

The LSTM post-processor makes a significant improvement over the NWM for several signatures. The improvement of runoff ratio, which is the fraction of precipitation that makes it through the stream gauge at the surface, could be a compensation for the uncalibrated soil parameters mentioned by Salas *et al.* (2018). The LSTM post-processor improves both high and low flow representations (5% & 95% flow quantiles), which are important for natural resources

Submitted to the Journal of The American Water Resources Association (JAWRA)

management. The mean daily discharge is the best represented hydrologic signature by all models. This is not surprising in terms of the LSTM and LSTM post-processor, because they were both trained to predict the mean daily discharge. It is also likely that the NWM calibrations, although not done at each basin, used mean daily discharge in the objective function.

The LSTM post-processor makes a significant improvement over the LSTM for baseflow index. This is the only signature which the LSTM post-processor improves both the NWM and the LSTM. This signature estimates the contribution of baseflow to the total discharge, which is computed by hydrograph separation. Klemeš (1986) (summarizing Lindsly's Applied Hydrology) cautions strongly against using hydrograph separation, because there is no real basis for distinguishing the source of flow in a stream. Even if the baseflow index is only a coarse approximation of flow sources, the ability of the LSTM to improve on the representation, and even further by the LSTM post-processor, there are still some hydrologic conditions being represented.

Results comparing calibrated basins vs. uncalibrated basins

The results in Table 6 shows the results of an analysis designed to replicate prediction in ungauged basins. The table has metrics from the NWM, LSTM and the LSTM post-processor predictions, as well as a comparison of the difference between the metrics of the LSTM models and the NWM. The difference between LSTM and NWM shows the magnitude of performance improvement or detriment at each basin, as does the difference between the LSTM post-processor and NWM. The mean NSE difference between the LSTM post-processor and NWM is negative, but the median difference is positive with the same magnitude as the LSTM. This indicates that the post-processor does not benefit the NWM in ungauged basins where the NWM makes poor predictions.

Submitted to the Journal of The American Water Resources Association (JAWRA)

TABLE 6. Performance of the LSTM and the LSTM post processor split between basins calibrated and uncalibrated in NWM version 2.0 retrospective. The rows with the pinkish fill indicate no significant difference between the calibrated and uncalibrated basin samples.

Nash-Sutcliffe Efficiency								
	Calibrated basins				Uncalibrated basins			
	mean	median	max	min	mean	median	max	min
NWM	0.47	0.60	0.94	-10.86	0.16	0.49	0.78	-8.58
LSTM	0.66	0.73	0.92	-1.33	0.51	0.65	0.87	-2.32
PP	0.67	0.75	0.93	-2.34	0.03	0.61	0.85	-19.59
LSTM - NWM	0.36	0.11	6.27	-0.67	0.19	0.10	10.20	-0.81
PP - NWM	-0.12	0.11	2.50	-11.01	0.20	0.12	8.52	-0.81
Total bias								
	Calibrated basins				Uncalibrated basins			
	mean	median	max	min	mean	median	max	min
NWM	0.02	-0.01	2.58	-0.65	0.01	-0.05	2.05	-0.56
LSTM	0.03	0.02	0.95	-0.19	0.08	0.03	1.04	-0.20
PP	0.01	0.00	0.91	-0.22	0.07	-0.04	3.43	-0.37
LSTM - NWM	0.02	0.02	1.11	-2.29	0.07	0.06	1.13	-1.00
PP - NWM	0.00	0.01	0.55	-1.67	0.06	0.00	1.63	-0.36
Peak timing error								
	Calibrated basins				Uncalibrated basins			
	mean	median	max	min	mean	median	max	min
NWM	1.07	0.92	3.00	0.16	1.00	0.77	2.88	0.15
LSTM	0.54	0.48	1.72	0.07	0.60	0.52	1.59	0.08
LSTM+NWM	0.54	0.42	1.78	0.04	0.60	0.44	1.86	0.08
LSTM - NWM	-0.53	-0.44	0.40	-2.07	-0.41	-0.40	0.16	-1.85
PP - NWM	-0.53	-0.44	0.48	-2.29	-0.40	-0.36	0.32	-1.50

Note: Pink rows indicate no significant difference between calibrated and uncalibrated basin samples.

The NWM, LSTM and the LSTM post-processor have higher NSE scores in calibrated basins than the uncalibrated basins. Note that these results are from the LSTM (and LSTM post-processor) trained on only the calibrated basins. In the case of the LSTM post-processor the mean NSE in uncalibrated basins is very low (0.03). This is a result of outlier basins weighing

Submitted to the Journal of The American Water Resources Association (JAWRA)

heavily on the mean. The table also shows that the median value of the LSTM post-processor is higher than the NWM, as is the maximum NSE value, but the minimum value is exceptionally low.

The total bias in calibrated basins is generally better than the uncalibrated basins. The timing error of the NWM is actually better in the uncalibrated basins, but the LSTM and LSTM post-processor both have better performance in the calibrated basins. The NSE values for the NWM, LSTM and the LSTM post-processor are significantly different in the calibrated basins vs. the uncalibrated basins, as are the differences between the LSTM and LSTM post-processor as compared to the NWM. The bias values are distinct between the two samples, but the differences between LSTM and LSTM post-processor vs. the NWM are not statistically distinct.

LSTM trained with only NWM states and fluxes.

Here we test the hypothesis that the NWM extracts enough information from the atmospheric forcings to make predictions that are as accurate as the LSTM. Figure 10 shows the results from the LSTM model with a variety of different inputs. The best performing LSTM models are trained with the five atmospheric forcing variables (with and without the NWM states and fluxes). This implies that LSTM extracted more information from the atmospheric forcings (and translated that information to streamflow predictions) than the NWM. The LSTM trained with the NWM states and fluxes only made better average daily streamflow predictions than the NWM itself in terms of overall NSE score and peak timing, but the NWM had a better overall bias. Of course, one of the NWM fluxes is the prediction of streamflow. The prediction of streamflow from the LSTM trained only with the NWM states as dynamic inputs still had higher (slightly, but significantly) mean NSE score, significantly lower peak timing error, but

Submitted to the Journal of The American Water Resources Association (JAWRA)

significantly higher bias. These plots show that the NWM has more poor performing basins than the LSTM trained only with the NWM states as dynamic inputs.

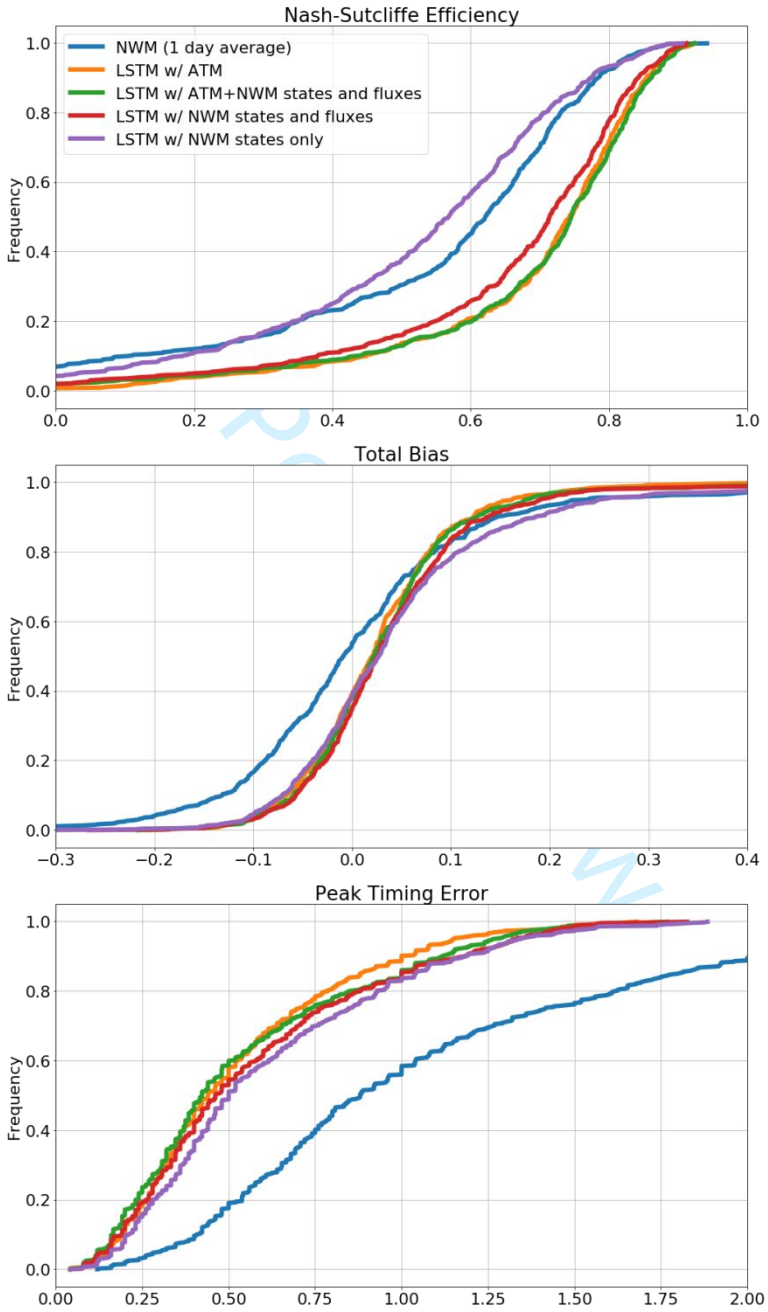

Submitted to the Journal of The American Water Resources Association (JAWRA)

FIGURE 10. Performance of the LSTM trained with different sets of dynamic inputs. The best performing models are trained with the five atmospheric forcing variables (orange and green). When trained with only NWM states and fluxes (red) the performance is better than the NWM. With trained with only the NWM states (purple) as dynamic inputs the prediction of streamflow is sometimes better and sometimes worse than the NWM itself (blue).

DISCUSSION

Potential for improving the performance of both the National Water Model and machine learning

Results presented here show that the LSTM post-processor has potential to improve the daily averaged flow predictions of the NWM. The LSTM post-processor provided significant benefit to the NWM streamflow predictions at almost all (93%) of the 531 basins analyzed here. In the few basins where this was not the case, it may be possible to use fine tuning to calibrate a version of the post-processor that is specific to each gauge location (as would be done in traditional model calibration), however the LSTM post-processor used here can be applied to any basin, even ungauged. Right now, the post-processor is trained on naturalized basins, so further work would be needed to include reservoirs and other management practices. It is worth noting that the computational cost of training the LSTM post-processor is many orders of magnitude lower than parameter estimation in a distributed model like the NWM, and the computational cost of forward prediction is negligible. Both training and prediction over all 531 basins used here can be done on a laptop in a few hours, if necessary (we used a small GPU cluster).

The NWM performance and the performance improvement from the LSTM post-processor were negatively correlated: basins with low performance by the NWM have the highest performance change from the LSTM post-processor. This means that post-processing can be expected to correct situations where the NWM gives very bad predictions. Conversely, the

Submitted to the Journal of The American Water Resources Association (JAWRA)

performance of the NWM and the LSTM (without NWM inputs) were not correlated. Considering also that the overall performance of the LSTM changed only minimally from the addition of the NWM inputs and that the LSTM still preferred to extract more information from precipitation forcings, we might conclude that the LSTM post-processor learned a new representation of the rainfall-runoff response. The overall improvement in the representation of hydrologic signatures indicates this new rainfall-runoff response is a better representation of physical flow patterns than either the NWM or the LSTM. The interpretation of the integrated gradient and the correlations between improvement and NWM features indicate that this improvement of flow patterns comes from information in the NWM representation of streamflow and snow states.

Application to real-time forecasting

The NWM is not simply a rainfall-runoff simulator; it simulates flow through 2.7 million river reaches around CONUS, dam operations, land surface processes, hydraulics, and other complications of large domain hydrology. The nature of the CAMELS catchments selected in these experiments are such that they have few engineered control structures, and are under 20,000 km^2. The results presented in this paper show that the LSTM post-processor improved streamflow predictions in similarly undisturbed catchments. Kratzert *et al.* (2019) show that these predictions extend into ungauged basins. Our results (section "*Results comparing calibrated basins vs. uncalibrated basins*") show that this is true for all but the poorest performing NWM basins. The immediate potential for improving real-time forecasting could be deploying this post-processor in undisturbed catchments, and undisturbed sub-catchments upstream of unnatural hydrologic conditions such as dams, agriculture lands and urban centers. An immediate next step would be to develop a post-processor that aggregates surface and

Submitted to the Journal of The American Water Resources Association (JAWRA)

subsurface runoff, and allows for the NWM router to aggregate these fluxes into streamflow. This would allow for retaining conceptual representations of lakes and reservoirs that already exist in the NWM.

Moving forward with theory-guided machine learning

The post-processing procedure presented here is one of the cruder techniques currently available for combining process-based and data-driven models. Several other methods of combining the benefits of machine learning (predictability) with the benefits of physically realistic hydrologic theory (robustness) are in development. For example, Pelissier *et al.* (2019) use Gaussian Processes to predict error between modeled and observed soil moisture, which allows ML to be used dynamically within a land surface model to correct the soil moisture state at each timestep of a simulation. Another example is using physical principles to constrain the loss function of an ML model during training. Implementing post-processing is relatively straightforward compared to other techniques such as adding physics into ML code or using ML to dynamically update the state variables.

DATA AVAILABILITY

All data and code used in this paper are publicly available in the following locations:
U.S. National Water Model: https://docs.opendata.aws/nwm-archive/readme.html
CAMELS data: https://ral.ucar.edu/solutions/products/camels
Data processing code: https://github.com/jmframe/nwm-reanalysis-model-data-processing
LSTM code: https://github.com/kratzert/ealstm_regional_modeling
Post-processing and analysis code: https://github.com/jmframe/nwm-post-processing-with-lstm

ACKNOWLEDGEMENTS

Authors from Johannes Kepler University were partially supported by a Google faculty research award. Jonathan Frame from the University of Alabama was partially supported by the NASA Terrestrial Hydrology Program. Grey Nearing from the University of Alabama was partially supported by the NCAR COMET program on a cooperative award with the National Water Center.

LITERATURE CITED

Addor, N., A.J. Newman, N. Mizukami, and M. P. Clark, 2017. The CAMELS Data Set: Catchment Attributes and Meteorology for Large-Sample Studies. Earth Syst. Sci 21: 5293–5313. https://doi.org/10.5194/hess-21-5293-2017.

Addor, N., G. Nearing, C. Prieto, A. J. Newman, N. Le Vine, and M. P. Clark, 2018. A Ranking of Hydrological Signatures Based on Their Predictability in Space. Water Resources Research 54, no. 11: 8792–8812. https://doi.org/10.1029/2018WR022606.

Chadalawada, J., H. M.V.V. Herath, and V. Babovic, 2020. Hydrologically Informed Machine Learning for Rainfall-Runoff Modeling: A Genetic Programming-Based Toolkit for Automatic Model Induction. Water Resources Research 56, no. 4: 1–23. https://doi.org/10.1029/2019WR026933.

Cosgrove, B, D. Gochis, E. P. Clark, Z. Cui, A. L. Dugger, G. M. Fall, X. Feng, M. A. Fresch, J. J. Gourley, S. Khan, D. Kitzmiller, H. S. Lee, Y. Liu, J. L. McCreight, A. J. Newman, A. Oubeidillah, L. Pan, C. Pham, F. Salas, K. M. Sampson, M. Smith, G. Sood, A. Wood, D. N. Yates, W. Yu and Y. Zhang, 2015. Hydrologic Modeling at the National Water Center: Operational Implementation of the WRF-Hydro Model to Support National Weather Service Hydrology. In AGU Fall Meeting Abstracts.

Daw, A., R. Q. Thomas, C. C. Carey, J. S. Read, A. P. Appling, and Anuj Karpatne, 2020. Physics-Guided Architecture (PGA) of Neural Networks for Quantifying Uncertainty in Lake Temperature Modeling. Proceedings of the 2020 SIAM International Conference on Data Mining, 532–40. https://doi.org/10.1137/1.9781611976236.60.

Elmer, N. J, 2019. Using Satellite Observations of River Height and Vegetation To Improve National Water Model Initialization and Streamflow Prediction. PhD diss., The University of Alabama in Huntsville.

Gauch, M., J. Mai, and J. Lin, 2019. The Proper Care and Feeding of CAMELS: How Limited Training Data Affects Streamflow Prediction 2342: 0–2. http://arxiv.org/abs/1911.07249.

Gupta, H. V., T. Wagener, and Y. Liu, 2008. Reconciling Theory with Observations: Elements of a Diagnostic Approach to Model Evaluation. Hydrological Processes 2274, no. November 2008: 2267–74. https://doi.org/10.1002/hyp.6989.

Gupta, H. V., H. Kling, K. K. Yilmaz, and G. F. Martinez, 2009. Decomposition of the Mean Squared Error and NSE Performance Criteria: Implications for Improving Hydrological Modelling. Journal of Hydrology 377, no. 1–2: 80–91. https://doi.org/10.1016/j.jhydrol.2009.08.003.

Hansen, C., J. S. Shiva, S. McDonald, and A. Nabors, 2019. Assessing Retrospective National Water Model Streamflow with Respect to Droughts and Low Flows in the Colorado River Basin. Journal of the American Water Resources Association 55, no. 4: 964–75. https://doi.org/10.1111/1752-1688.12784.

Hochreiter, S, 1991. "Untersuchungen Zu Dynamischen Neuronalen Netzen." Doctoral diss., Institut Für Informatik, Technische Universität, Munchen http://people.idsia.ch/~juergen/SeppHochreiter1991ThesisAdvisorSchmidhuber.pdf.

Hochreiter, S., and J. Schmidhuber, 1997. Long Short-Term Memory. Neural Computation 9, no. 8: 1735–80. https://doi.org/10.1162/neco.1997.9.8.1735.

Karpatne, A., W. Watkins, J. Read, and V. Kumar, 2017a. Physics-Guided Neural Networks (PGNN): An Application in Lake Temperature Modeling. http://arxiv.org/abs/1710.11431.

Karpatne, A., G. Atluri, J. H. Faghmous, M. Steinbach, A. Banerjee, A. Ganguly, S. Shekhar, N. Samatova, and V. Kumar, 2017b. Theory-Guided Data Science: A New Paradigm for Scientific Discovery from Data. IEEE Transactions on Knowledge and Data Engineering 29, no. 10: 2318–31. https://doi.org/10.1109/TKDE.2017.2720168.

Kim, J., L. Read, L. E. Johnson, D. Gochis, R. Cifelli, and H. Han, 2020. An Experiment on Reservoir Representation Schemes to Improve Hydrologic Prediction: Coupling the National Water Model with the HEC-ResSim. Hydrological Sciences Journal 0, no. 0: 1. https://doi.org/10.1080/02626667.2020.1757677.

Klemeš, V, 1986. Dilettantism in Hydrology: Transition or Destiny? Water Resources Research 22, no. 9 S: 177S-188S. https://doi.org/10.1029/WR022i09Sp0177S.

Kratzert, F., D. Klotz, C. Brenner, K. Schulz, and M. Herrnegger, 2018. Rainfall–Runoff Modelling Using Long Short-Term Memory (LSTM) Networks. Hydrology and Earth System Sciences 22, no. 11: 6005–22. https://doi.org/10.5194/hess-22-6005-2018.

Kratzert, F., D. Klotz, M. Herrnegger, A. K. Sampson, S. Hochreiter, and G. S. Nearing, 2019a. Towards Improved Predictions in Ungauged Basins: Exploiting the Power of Machine Learning. Water Resources Research, 2019WR026065. https://doi.org/10.1029/2019WR026065.

Kratzert, F., D. Klotz, G. Shalev, G. Klambauer, S. Hochreiter, and G. S. Nearing, 2019b. Towards Learning Universal, Regional, and Local Hydrological Behaviors via Machine Learning Applied to Large-Sample Datasets. Hydrology and Earth System Sciences 23, no. 12: 5089–5110. https://doi.org/10.5194/hess-23-5089-2019.

Newman, A. J., M. P. Clark, K. Sampson, A. Wood, L. E. Hay, A. Bock, R. J. Viger, D. Blodgett, L. Brekke, J. R. Arnold, T. Hopson, and Q. Duan, 2015. Development of a Large-Sample Watershed-Scale Hydrometeorological Data Set for the Contiguous USA: Data Set Characteristics and Assessment of Regional Variability in Hydrologic Model Performance. Hydrology and Earth System Sciences 19, no. 1: 209–23. https://doi.org/10.5194/hess-19-209-2015.

Pelissier, C., J. Frame, and G. Nearing, 2019. Combining Parametric Land Surface Models with Machine Learning. arXiv preprint arXiv:2002.06141.

Reichstein, M., G. Camps-valls, B. Stevens, M. Jung, J. Denzler, and N. Carvalhais, 2019. Deep Learning and Process Understanding for Data-Driven Earth System Science. Nature 566: 195–204. https://doi.org/10.1038/s41586-019-0912-1.

Ritter, A., and R. Muñoz-Carpena, 2013. Performance Evaluation of Hydrological Models: Statistical Significance for Reducing Subjectivity in Goodness-of-Fit Assessments. Journal of Hydrology 480: 33–45. https://doi.org/10.1016/j.jhydrol.2012.12.004.

Salas, F. R., M. A. Somos-Valenzuela, A. Dugger, D. R. Maidment, D. J. Gochis, C. H. David, W. Yu, D. Ding, E. P. Clark, and N. Noman, 2018. Towards Real-Time Continental Scale Streamflow Simulation in Continuous and Discrete Space. Journal of the American Water Resources Association 54, no. 1: 7–27. https://doi.org/10.1111/1752-1688.12586.

Steiger, J., and M. Browne, 1984. The Comparison of Interdependent Correlations between Optimal Linear Composites. Psychometrika 49, no. 1: 11–24. https://doi.org/10.1017/CBO9781107415324.004.

Sundararajan, M., A. Taly, and Q. Yan, 2017. Axiomatic Attribution for Deep Networks. 34th International Conference on Machine Learning, ICML 2017 7: 5109–18.

Tartakovsky, A. M., C. O. Marrero, P. Perdikaris, G. D. Tartakovsky, and D. Barajas-Solano, 2020. Physics-Informed Deep Neural Networks for Learning Parameters and Constitutive Relationships in Subsurface Flow Problems. Water Resources Research 56, no. 5: 1–16. https://doi.org/10.1029/2019WR026731.

Xia, Y., K. Mitchell, M. Ek, J. Sheffield, B. Cosgrove, E. Wood, L. Luo, C. Alonge, H. Wei, J. Meng, B. Livneh, D. Lettenmaier, V. Koren, Q. Duan, K. Mo, Y. Fan, and D. Mocko, 2012. Continental-Scale Water and Energy Flux Analysis and Validation for the North American Land Data Assimilation System Project Phase 2 (NLDAS-2): 1. Intercomparison and Application of Model Products. Journal of Geophysical Research Atmospheres 117, no. 3. https://doi.org/10.1029/2011JD016048.

Ye, A., Q. Duan, X. Yuan, E. F Wood, and J. Schaake, 2014. Hydrologic Post-Processing of MOPEX Streamflow Simulations. Journal of Hydrology 508: 147–56. https://doi.org/10.1016/j.jhydrol.2013.10.055.